

Search for dark matter annual modulation with DarkSide-50

P. Agnes,¹ I.F.M. Albuquerque,² T. Alexander,³ A.K. Alton,⁴ M. Ave,² H.O. Back,³ G. Batignani,^{5,6} K. Biery,⁷ V. Bocci,⁸ W.M. Bonivento,⁹ B. Bottino,^{10,11} S. Bussino,^{12,13} M. Cadeddu,⁹ M. Cadoni,^{14,9} F. Calaprice,¹⁵ A. Caminata,¹¹ M.D. Campos,¹⁶ N. Canci,¹⁷ M. Caravati,⁹ N. Cargioli,⁹ M. Cariello,¹¹ M. Carlini,^{17,18} V. Cataudella,^{19,20} P. Cavalcante,^{21,17} S. Cavuoti,^{19,20} S. Chashin,²² A. Chepurinov,²² C. Cicalò,⁹ G. Covone,^{19,20} D. D'Angelo,^{23,24} S. Davini,¹¹ A. De Candia,^{19,20} S. De Cecco,^{8,25} G. De Filippis,^{19,20} G. De Rosa,^{19,20} A.V. Derbin,²⁶ A. Devoto,^{14,9} M. D'Incecco,¹⁷ C. Dionisi,^{8,25} F. Dordei,⁹ M. Downing,²⁷ D. D'Urso,^{28,29} M. Fairbairn,¹⁶ G. Fiorillo,^{19,20} D. Franco,³⁰ F. Gabriele,⁹ C. Galbiati,^{15,18,17} C. Ghiano,¹⁷ C. Giganti,³¹ G.K. Giovanetti,¹⁵ A.M. Goretti,¹⁷ G. Grilli di Cortona,^{32,8} A. Grobov,^{33,34} M. Gromov,^{22,35} M. Guan,³⁶ M. Gulino,^{37,29} B.R. Hackett,³ K. Herner,⁷ T. Hessel,³⁰ B. Hosseini,⁹ F. Hubaut,³⁸ T. Hugues,³⁹ E.V. Hungerford,⁴⁰ An. Ianni,^{15,17} V. Ippolito,⁸ K. Keeter,⁴¹ C.L. Kendziora,⁷ M. Kimura,³⁹ I. Kochanek,¹⁷ D. Korabely,³⁵ G. Korga,^{40,17} A. Kubankin,⁴² M. Kuss,⁵ M. Kuźniak,³⁹ M. La Commara,^{19,20} M. Lai,^{14,9} X. Li,¹⁵ M. Lissia,⁹ G. Longo,^{19,20} O. Lychagina,^{35,22} I.N. Machulin,^{33,34} L.P. Mapelli,⁴³ S.M. Mari,^{12,13} J. Maricic,⁴⁴ A. Messina,^{8,25} R. Milincic,⁴⁴ J. Monroe,¹ M. Morrocchi,^{5,6} X. Mougeot,⁴⁵ V.N. Muratova,²⁶ P. Musico,¹¹ A.O. Nozdrina,^{33,34} A. Oleinik,⁴² F. Ortica,^{46,47} L. Pagani,⁴⁸ M. Pallavicini,^{10,11} L. Pandola,²⁹ E. Pantic,⁴⁸ E. Paoloni,^{5,6} K. Pelczar,^{17,49} N. Pelliccia,^{46,47} S. Piacentini,^{8,25} A. Pocar,²⁷ D.M. Poehlmann,⁴⁸ S. Pordes,⁷ S.S. Poudel,⁴⁰ P. Pralavorio,³⁸ D.D. Price,⁵⁰ F. Ragusa,^{23,24} M. Razeti,⁹ A. Razeto,¹⁷ A.L. Renshaw,⁴⁰ M. Rescigno,⁸ J. Rode,^{31,30} A. Romani,^{46,47} D. Sablone,^{15,17} O. Samoylov,³⁵ E. Sandford,⁵⁰ W. Sands,¹⁵ S. Sanfilippo,²⁹ C. Savarese,¹⁵ B. Schlitzer,⁴⁸ D.A. Semenov,²⁶ A. Shchagin,⁴² A. Sheshukov,³⁵ M.D. Skorokhvatov,^{33,34} O. Smirnov,³⁵ A. Sotnikov,³⁵ S. Stracka,⁵ Y. Suvorov,^{19,20} R. Tartaglia,¹⁷ G. Testera,¹¹ A. Tonazzo,³⁰ E.V. Unzhakov,²⁶ A. Vishneva,³⁵ R.B. Vogelaar,²¹ M. Wada,^{39,14} H. Wang,⁴³ Y. Wang,^{43,36} S. Westerdale,⁵¹ M.M. Wojcik,⁴⁹ X. Xiao,⁴³ C. Yang,³⁶ and G. Zuzel⁴⁹

(The DarkSide-50 Collaboration)

¹*Department of Physics, Royal Holloway University of London, Egham TW20 0EX, UK*

²*Instituto de Física, Universidade de São Paulo, São Paulo 05508-090, Brazil*

³*Pacific Northwest National Laboratory, Richland, WA 99352, USA*

⁴*Physics Department, Augustana University, Sioux Falls, SD 57197, USA*

⁵*INFN Pisa, Pisa 56127, Italy*

⁶*Physics Department, Università degli Studi di Pisa, Pisa 56127, Italy*

⁷*Fermi National Accelerator Laboratory, Batavia, IL 60510, USA*

⁸*INFN Sezione di Roma, Roma 00185, Italy*

⁹*INFN Cagliari, Cagliari 09042, Italy*

¹⁰*Physics Department, Università degli Studi di Genova, Genova 16146, Italy*

¹¹*INFN Genova, Genova 16146, Italy*

¹²*INFN Roma Tre, Roma 00146, Italy*

¹³*Mathematics and Physics Department, Università degli Studi Roma Tre, Roma 00146, Italy*

¹⁴*Physics Department, Università degli Studi di Cagliari, Cagliari 09042, Italy*

¹⁵*Physics Department, Princeton University, Princeton, NJ 08544, USA*

¹⁶*Physics, Kings College London, Strand, London WC2R 2LS, UK*

¹⁷*INFN Laboratori Nazionali del Gran Sasso, Assergi (AQ) 67100, Italy*

¹⁸*Gran Sasso Science Institute, L'Aquila 67100, Italy*

¹⁹*Physics Department, Università degli Studi "Federico II" di Napoli, Napoli 80126, Italy*

²⁰*INFN Napoli, Napoli 80126, Italy*

²¹*Virginia Tech, Blacksburg, VA 24061, USA*

²²*Skobel'syn Institute of Nuclear Physics, Lomonosov Moscow State University, Moscow 119234, Russia*

²³*Physics Department, Università degli Studi di Milano, Milano 20133, Italy*

²⁴*INFN Milano, Milano 20133, Italy*

²⁵*Physics Department, Sapienza Università di Roma, Roma 00185, Italy*

²⁶*Saint Petersburg Nuclear Physics Institute, Gatchina 188350, Russia*

²⁷*Amherst Center for Fundamental Interactions and Physics*

Department, University of Massachusetts, Amherst, MA 01003, USA

²⁸*Chemistry and Pharmacy Department, Università degli Studi di Sassari, Sassari 07100, Italy*

²⁹*INFN Laboratori Nazionali del Sud, Catania 95123, Italy*

- ³⁰APC, Université de Paris, CNRS, Astroparticule et Cosmologie, Paris F-75013, France
- ³¹LPNHE, CNRS/IN2P3, Sorbonne Université, Université Paris Diderot, Paris 75252, France
- ³²INFN Laboratori Nazionali di Frascati, Frascati 00044, Italy
- ³³National Research Centre Kurchatov Institute, Moscow 123182, Russia
- ³⁴National Research Nuclear University MEPhI, Moscow 115409, Russia
- ³⁵Joint Institute for Nuclear Research, Dubna 141980, Russia
- ³⁶Institute of High Energy Physics, Beijing 100049, China
- ³⁷Engineering and Architecture Faculty, Università di Enna Kore, Enna 94100, Italy
- ³⁸Centre de Physique des Particules de Marseille, Aix Marseille Univ, CNRS/IN2P3, CPPM, Marseille, France
- ³⁹AstroCeNT, Nicolaus Copernicus Astronomical Center, 00-614 Warsaw, Poland
- ⁴⁰Department of Physics, University of Houston, Houston, TX 77204, USA
- ⁴¹School of Natural Sciences, Black Hills State University, Spearfish, SD 57799, USA
- ⁴²Radiation Physics Laboratory, Belgorod National Research University, Belgorod 308007, Russia
- ⁴³Physics and Astronomy Department, University of California, Los Angeles, CA 90095, USA
- ⁴⁴Department of Physics and Astronomy, University of Hawai'i, Honolulu, HI 96822, USA
- ⁴⁵Université Paris-Saclay, CEA, List, Laboratoire National Henri Becquerel (LNE-LNHB), F-91120 Palaiseau, France
- ⁴⁶Chemistry, Biology and Biotechnology Department, Università degli Studi di Perugia, Perugia 06123, Italy
- ⁴⁷INFN Perugia, Perugia 06123, Italy
- ⁴⁸Department of Physics, University of California, Davis, CA 95616, USA
- ⁴⁹M. Smoluchowski Institute of Physics, Jagiellonian University, 30-348 Krakow, Poland
- ⁵⁰The University of Manchester, Manchester M13 9PL, United Kingdom
- ⁵¹Department of Physics and Astronomy, University of California, Riverside, CA 92507, USA
- (Dated: 17th July, 2023)

Dark matter induced event rate in an Earth-based detector is predicted to show an annual modulation as a result of the Earth's orbital motion around the Sun. We searched for this modulation signature using the ionization signal of the DarkSide-50 liquid argon time projection chamber. No significant signature compatible with dark matter is observed in the electron recoil equivalent energy range above 40 eV_{ee} , the lowest threshold ever achieved in such a search.

The combined effect of Earth's rotations around the Sun and the galactic center is expected to produce an annual modulation of the dark matter particle interaction rate in terrestrial detectors [1], thereby offering a unique signature for directly probing dark matter particles and unveiling their true nature. The DAMA/LIBRA experiment claimed the detection of such a signature in their NaI detectors in the keV range [2, 3]. The interpretation of this claim with the Weakly Interacting Massive Particle (WIMP) hypothesis is however currently facing challenges due to the null detection of WIMP-induced nuclear-recoil signals in other experiments [4–12]. An independent approach to test this claim and possibly to reveal WIMP properties can be offered by searching for the modulation with other detectors which have different target materials, background sources, energy resolution, and experimental sites.

Dual-phase noble-liquid time projection chambers (TPCs) measure the scintillation and ionization signals from a particle interacting in the liquid. Such detectors were originally designed to discover and have led the search for the WIMPs with masses above $10\text{ GeV}/c^2$. Moreover, in the last decade, they have also exhibited world-class sensitivity to light dark matter candidates exploiting only the ion-

ization signal spectrum above a few detected ionization electrons (N_e) [13–21]. Among them, the DarkSide-50 detector, a liquid argon (LAr) TPC located underground at the Laboratori Nazionali del Gran Sasso (LNGS) [7, 22, 23], recently demonstrated an unprecedented sensitivity in this energy region [24–27]. This achievement was accomplished by looking for an event excess in the energy spectrum with respect to the background model above $0.06\text{ keV}_{\text{ee}}$ electron recoil equivalent (keV_{ee}). In this work, we report for the first time on the search for the annual rate modulation of events down to $0.04\text{ keV}_{\text{ee}}$, the lowest threshold ever achieved in a dark matter modulation search. The analysis relies on two approaches: the maximum likelihood fit and the Lomb-Scargle periodogram. The results are also compared to the claim by the DAMA/LIBRA experiment.

The DarkSide-50 TPC is housed in a stainless steel double-walled, vacuum-insulated cryostat, shielded by a 30 t boron-loaded liquid scintillator veto instrumented with 110 8-inch PMTs. The purpose of this is to actively tag neutrons *in situ*. A 1 kt water Čerenkov veto, equipped with 80 PMTs, surrounds the neutron veto to actively tag cosmic muons and to passively shield the TPC against external back-

grounds [28].

Two arrays of 19 3-inch photomultiplier tubes (PMTs), located at the top and the bottom of the TPC, detect light pulses from scintillation (S1) induced by particle interactions in the liquid bulk. The same interactions generate ionization electrons, which are drifted through the LAr volume by a 200 V/cm electric field up to the top of the TPC. Then, they are extracted into the gas phase by a 2.8 kV/cm field and induce delayed photon pulses (S2) by electroluminescence under a 4.2 kV/cm field.

DarkSide-50 started taking data on April 2015 with a low-radioactivity LAr target, extracted from a deep underground source (UAr) [23], and concluded the operations on February 2018. The first four months of data were contaminated by the cosmogenic ^{37}Ar isotope, with a half-life of 35.0 d [29], and were only used to calibrate the ionization response [30]. About 25% of the rest of the data taking was devoted to calibration campaigns with dissolved and external radioactive sources. The livetime used in this paper corresponds to 693.3 d.

Selected events are required to be single-scatter, *i.e.*, with a single S2 pulse, after a veto of 20 ms for each event triggering the DAQ. Additional cuts are used to remove pileup pulses, surface α events, and events reconstructed in the outer ~ 7 cm thick cylindrical shell of the TPC. In addition, the low energy threshold for this analysis is defined in order to reject spurious electrons (SEs) [17, 24], the object of a paper in preparation. These originate from ionization electrons trapped on impurities along the drift in LAr, and released with a certain delay. A full description of the selection criteria can be found in Ref. [24].

A crucial aspect for this analysis is long-term stability of the detector performance, monitored by various sensors incorporated inside the cryogenic system, as well as by the recorded events from the TPC itself. The two parameters whose fluctuations may potentially have a high impact on the modulation search are the electric drift field, F , and the average number of detected S2 photons per ionization electron extracted in the gas phase, g_2 . The stability of F is monitored *ex situ* via the stability of the supplied high voltages for the electric fields and *in situ* via the stability of the drift time of events at the very bottom of the TPC. The maximum fluctuation of F was estimated to be less than 0.01%, too small to affect the ionization response. Based on the S2/S1 ratio for electronic recoil events above the region of interest (RoI) (0.04–21 keV_{ee}), g_2 varies at most by 0.5% over the whole data-taking period. The impact from the instability is evaluated by pseudo experi-

ments and found to be negligible compared to the statistical fluctuations.

The time evolution of background events can be described by the combination of a set of decaying exponentials and a constant term. The latter component includes the radioactive backgrounds whose lifetime is much longer than the data-taking period of about three years, and is dominated by the β -decay of ^{39}Ar (268 yr [31]). The exponential components arise from the decays of ^{37}Ar (35.0 d [29]), ^{85}Kr (10.8 yr [32]), ^{54}Mn (312.1 d [32]), and ^{60}Co (5.27 yr [33]). The first two isotopes are intrinsically present in the LAr, while the latter two are contaminants of the PMTs, and ^{60}Co is also present in the cryostat stainless steel. The latter two emit γ - and x-rays, which deposit energy in the LAr target. The background model is generated with the DarkSide-50 **Geant4**-based Monte Carlo [34] code. The model is built on data from an extensive materials screening campaign to characterize the trace radioactivity content of every detector component. It also uses *in situ* measurements with DarkSide-50 [24] and incorporates the detector response model [30].

Fig. 1 shows the measured time-dependent event rates for events with N_e in the 4–41 e^- and 41–68 e^- ranges, corresponding to 0.06–2.0 keV_{ee} and 2.0–6.0 keV_{ee}, respectively. The signal and backgrounds are modelled with

$$f(t) = A_\chi \cos\left(\frac{t - \phi}{T/2\pi}\right) + \sum_l \frac{A_l}{\tau_l} e^{-t/\tau_l} + C, \quad (l = ^{37}\text{Ar}, ^{85}\text{Kr}, ^{54}\text{Mn}, ^{60}\text{Co}) \quad (1)$$

where A_χ is the amplitude of the modulated term of the signal, ϕ the phase, and T the period fixed to 1 yr. The constant term C is the sum of the time-averaged signal component and long-lived backgrounds. The parameters τ_l and A_l correspond to the decay times and amplitudes, respectively, of the short-lived isotopes l . Examples of background-only fits to data, by fixing $A_\chi = 0$, are shown in Fig. 1 for the two ranges.

The statistical significance of a possible modulated signal is assessed using the following binned likelihood with the bin width of 7 d

$$\mathcal{L} = \prod_{i \in t_{\text{bins}}} \mathcal{P}(n_i | m_i(A_\chi, \phi, C, \Theta)) \times \prod_{\theta_k \in \Theta} \mathcal{G}(\theta_k | \theta_k^0, \Delta\theta_k). \quad (2)$$

The first term represents the Poisson probability of observing n_i events in the i^{th} time bin with respect to the expected ones, $m_i(A_\chi, \phi, C, \Theta)$, evaluated with Eq. (1). In the fit, A_χ , ϕ and C are

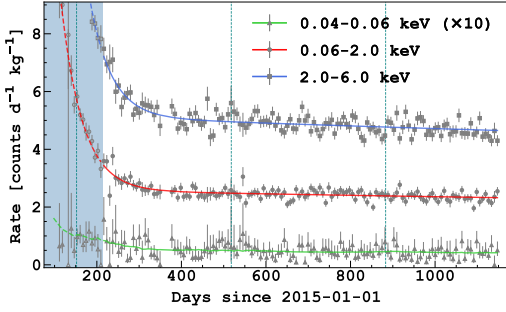


FIG. 1. Temporal evolution of the observed event rates for $3\text{--}4 e^-$ (corresponding to $0.04\text{--}0.06 \text{ keV}_{ee}$), $4\text{--}41 e^-$ ($0.06\text{--}2.0 \text{ keV}_{ee}$), and $41\text{--}68 e^-$ ($2.0\text{--}6.0 \text{ keV}_{ee}$) ranges. The bin width is 7 d. The coloured solid lines represent the background-only fit. The vertical dotted lines correspond to June 2nd, when the dark matter induced event rate has its maximum. The blue-shaded region corresponds to the first four months devoted to the detector calibration and is thus excluded from this analysis.

left free to vary, while the other parameters are contained inside Θ , which represents the set of remaining nuisance parameters constrained by the Gaussian penalty terms in the last factor of Eq. (2). In the latter, θ_k^0 and $\Delta\theta_k$ represent the nominal central values and uncertainties, respectively, of the nuisance parameters and are listed in Table I. The nuisance parameters account for uncertainties on the fiducial volume of the TPC (which induces a 1.1% uncertainty on the event rate from ^{54}Mn and ^{60}Co in the PMTs and cryostat; and a 1.5% uncertainty on the other event rates, acting in a correlated way [24]) and on the activities of short-lived decays in the energy range of interest. These are obtained from the combination of the uncertainty on the measured rate (14%, 4.7%, 40%, 12% for ^{37}Ar , ^{85}Kr , ^{54}Mn , ^{60}Co , respectively [24]), with the uncertainty arising from the definition of the energy range due to the ionization response. In addition, the uncertainty on the ^{85}Kr activity is combined with the spectral uncertainties from the β -decay Q-value and atomic exchange and screening effects [35, 36], as discussed in Ref. [24].

The fit to data with Eq. (2) does not show any evidence of modulation in either of the two analyzed ranges. Fig. 2 shows the best fit values of (A_χ, ϕ) , and the associated 68% and 95% confidence level (C.L.) contours, for the two energy ranges. The same analysis has been repeated by varying the bin width from 1 d to 10 d, and no significant variations have been found.

The result in the $2.0\text{--}6.0 \text{ keV}_{ee}$ range is used to test the modulation observed by DAMA/LIBRA in the same interval, compatible with a dark matter

TABLE I. List of the nuisance parameters, together with their central values (θ_k^0) and uncertainties ($\Delta\theta_k$). The uncertainties are given as percentages of the corresponding central values. The uncertainties arising from the β -decay spectrum and the ionization response are reported in terms of the event rate.

Parameter	θ_k^0	$\Delta\theta_k$	Refs.
T	1 yr	0	
Fiducial volume	19.4 kg	1.5%*	[24]
$\tau_{37\text{Ar}}$	35.0 d	0	[29]
$\tau_{85\text{Kr}}$	10.8 yr	0	[32]
$\tau_{54\text{Mn}}$	312.1 d	0	[32]
$\tau_{60\text{Co}}$	5.27 yr	0	[33]
$A_{37\text{Ar}}$	2.1 counts/(d kg) [†]	14%	
$A_{85\text{Kr}}$	1.7 counts/(d kg) [†]	4.7%	[24]
$A_{54\text{Mn}}$	0.02 counts/(d kg) [†]	40%	[24]
$A_{60\text{Co}}$	0.58 counts/(d kg) [†]	12%	[24]
^{85}Kr β -decay spectrum	1.7 counts/(d kg) [†]	0.7% [†]	[24, 35, 36]
Ionization response	4.4 counts/(d kg) [†]	0.4% [†]	[24, 30]

* More details in the text.

[†] In $2.0\text{--}6.0 \text{ keV}_{ee}$ range.

signal over 14 cycles with a significance of $>13\sigma$ [3]. The significance from this analysis is such that we can neither confirm nor reject the DAMA/LIBRA observation over the null hypothesis. For completeness, the same conclusion is drawn for the $1.0\text{--}3.0 \text{ keV}_{ee}$ range, also analyzed by DAMA/LIBRA.

Additional constraints on the modulation amplitude are obtained by simultaneously fitting event timestamps and energies after fixing the period (1 yr) and the phase (maximum at June 2nd) to those expected from the Standard Halo Model [41, 42]. This approach does not require any assumption on the SE rate and thus allows the range to be extended down to $3 e^-$ or 0.04 keV_{ee} , which corresponds to the primary electron induced by the interaction plus, on average, two subsequent ionization electrons. The likelihood,

$$\mathcal{L} = \prod_{i \in t_{\text{bins}}} \prod_{j \in E_{\text{bins}}} \mathcal{P}\left(n_i^j | m_i^j(A_\chi^j, C^j, \tilde{\Theta})\right) \times \prod_{\tilde{\theta}_k \in \tilde{\Theta}} \mathcal{G}(\tilde{\theta}_k | \tilde{\theta}_k^0, \Delta\tilde{\theta}_k), \quad (3)$$

is the product of the Poisson probabilities in each of the ij -bins defined by the event time (i) and energy expressed in terms of number of electrons (j) given the signal amplitude, A_χ^j , and the constant background component, C^j . The chosen bin width along the time axis corresponds to 7 d and the bin widths along the energy axis are 0.02 keV_{ee} below 0.06 keV_{ee} , 0.25 keV_{ee} below 1 keV_{ee} , 1 keV_{ee}

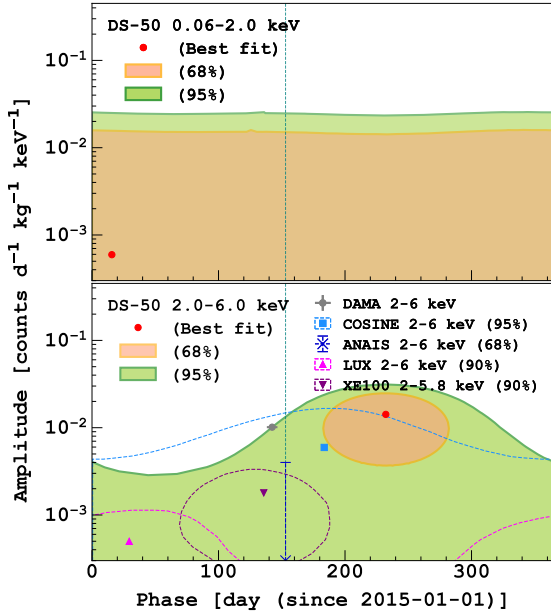


FIG. 2. Best fit parameters in the phase versus amplitude space from the likelihood analysis with the fixed period of 1 yr. The vertical dotted line represents the phase of the dark matter signal expected from the standard halo model. Also shown are the results from other experiments using NaI(Tl) crystal scintillators (DAMA/LIBRA [3], COSINE-100 [37], and ANAIS-112 [38]) and liquid xenon TPC (XENON100 [39] and LUX [40]).

up to 6 keV_{ee} , and 2 keV_{ee} elsewhere, starting from 0.04 keV_{ee} ($3 e^-$). The sample of events with $3 e^-$ is contaminated by SE's. To account for this background, we anchored its time variation to that of events below $3 e^-$, selected in coincidence with the previous event, largely dominated by SE. This approach is justified by the observation that the spectrum of events occurring in a 2 ms window from the previous event, which consists of more than 90% of SE's, is stable over time. The amplitude of the signal in each energy interval, A_{χ}^j , is assumed uncorrelated with the others. Nuisance parameters $\tilde{\Theta}$, in Eq. (3) are the same as in Eq. (2), but account for energy spectral distortions of the background components as done in Ref. [24].

Fig. 3 shows the best-fitted amplitude as a function of the energy, together with the 1- and 2- σ significance coverages, as derived with background-only Monte Carlo datasets. The results from DAMA/LIBRA [3], COSINE-100 [37], and XMASS [10] are also shown. In contrast to our approach, the DAMA/LIBRA looked at each energy bin independently and measured the amplitude by looking at the residuals of a yearly averaged event

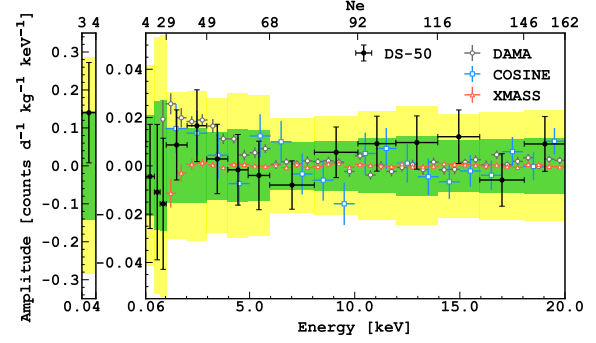


FIG. 3. Best fit amplitude of the modulation signal as a function of N_e . The green and yellow bands represent the expected 1σ and 2σ statistical fluctuations derived by background-only Monte Carlo samples. Also shown are the results from DAMA/LIBRA [3], COSINE-100 [37], and XMASS [10].

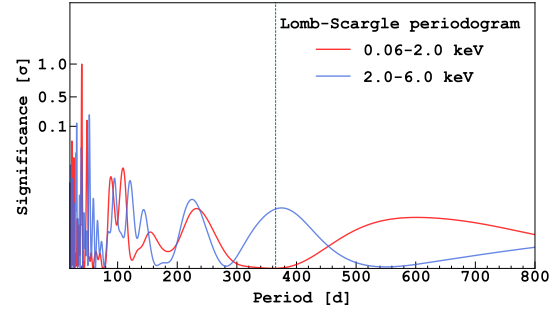


FIG. 4. Observed sinusoidal signal strengths from the Lomb-Scargle periodogram as a function of its period. The vertical axis is normalized by the 1σ false alarm probability. The vertical dashed line corresponds to the period of 1 yr.

rate.

Finally, a Lomb-Scargle periodogram analysis [43] is performed on the temporal evolution of the event rate to look for sinusoidal signals with any period, including the one expected from dark matter. The analysis is applied to the data residuals, after the subtraction of the best-fitted background model, shown in Fig. 1. The uncertainty from the background fit is propagated to the data errors. The false alarm probability is calculated with the Bootstrap method [43] and used to assess the significance of the sinusoidal signals. The sensitivity of this analysis is evaluated by applying the Lomb-Scargle analysis over 1000 pseudo experiments where an annual modulation signal has been injected. A median of 1σ significance for the false alarm probability is obtained with the addition of $0.03 \text{ counts}/(\text{d kg keV})$. The analysis of the data does not identify any significant modulation, scanning periods up to 800 d, as shown in Fig. 4.

In conclusion, we searched for an event rate modulation in the DarkSide-50 data between 2.0 and 6.0 keV_{ee}, where DAMA/LIBRA observed a yearly modulated signal compatible with dark matter. Also, for the first time, we probed the energy range down to 0.04 keV_{ee}, the lowest threshold ever probed in an annual dark-matter modulation search. In none of the analyzed intervals, a modulation signal was observed. The significance of this result is not sufficient to confirm or reject the DAMA/LIBRA observation.

The stability of the DarkSide-50 detector over nearly three years of operation, the accuracy of the background model, and the low-energy threshold achieved demonstrate the competitiveness of the dual-phase LAr-TPC technology in searching for modulation signals. This result is therefore promising in view of future massive dual-phase liquid argon experiments [44–46], expected to reach much larger exposures and even lower background levels.

The DarkSide Collaboration offers its profound gratitude to the LNGS and its staff for their invaluable technical and logistical support. We also thank the Fermilab Particle Physics, Scientific, and Core Computing Divisions. Construction and operation of the DarkSide-50 detector was supported by the U.S. National Science Foundation (NSF) (Grants No. PHY-0919363, No. PHY-1004072, No. PHY-1004054, No. PHY-1242585, No. PHY-1314483, No. PHY-1314501, No. PHY-1314507, No. PHY-1352795, No. PHY-1622415, and associated collaborative grants No. PHY-1211308 and No. PHY-1455351), the Italian Istituto Nazionale di Fisica Nucleare, the U.S. Department of Energy (Contracts No. DE-FG02-91ER40671, No. DEAC02-07CH11359, and No. DE-AC05-76RL01830), the Polish NCN (Grant No. UMO-2019/33/B/ST2/02884) and the Polish Ministry for Education and Science (Grant No. 6811/IA/SP/2018). We also acknowledge financial support from the French Institut National de Physique Nucléaire et de Physique des Particules (IN2P3), the IN2P3-COPIN consortium (Grant No. 20-152), and the UnivEarthS LabEx program (Grants No. ANR-10-LABX-0023 and No. ANR-18-IDEX-0001), from the São Paulo Research Foundation (FAPESP) (Grant No. 2016/09084-0), from the Interdisciplinary Scientific and Educational School of Moscow University “Fundamental and Applied Space Research”, from the Program of the Ministry of Education and Science of the Russian Federation for higher education establishments, project No. FZWG-2020-0032 (2019-1569), the International Research Agenda Programme AstroCeNT

(MAB/2018/7) funded by the Foundation for Polish Science (FNP) from the European Regional Development Fund, and the European Union’s Horizon 2020 research and innovation program under grant agreement No 952480 (DarkWave), and from the Science and Technology Facilities Council, United Kingdom. I. Albuquerque is partially supported by the Brazilian Research Council (CNPq). The theoretical calculation of beta decays was performed as part of the EMPIR Project 20FUN04 PrimA-LTD. This project has received funding from the EMPIR program co-financed by the Participating States and from the European Union’s Horizon 2020 research and innovation program. Isotopes used in this research were supplied by the United States Department of Energy Office of Science by the Isotope Program in the Office of Nuclear Physics.

-
- [1] A. K. Drukier, K. Freese, and D. N. Spergel, Detecting Cold Dark Matter Candidates, *Phys. Rev. D* **33**, 3495 (1986).
 - [2] R. Bernabei *et al.*, Final model independent result of DAMA/LIBRA-phase1, *Eur. Phys. J. C* **73**, 2648 (2013), [arXiv:1308.5109 \[astro-ph.GA\]](#).
 - [3] R. Bernabei *et al.*, Further results from DAMA/Libra-phase2 and perspectives, *Nucl. Phys. Atom. Energy* **22**, 329 (2021).
 - [4] D. S. Akerib *et al.* (LUX), Results from a search for dark matter in the complete LUX exposure, *Phys. Rev. Lett.* **118**, 021303 (2017), [arXiv:1608.07648 \[astro-ph.CO\]](#).
 - [5] R. Agnese *et al.* (SuperCDMS), Results from the Super Cryogenic Dark Matter Search Experiment at Soudan, *Phys. Rev. Lett.* **120**, 061802 (2018), [arXiv:1708.08869 \[hep-ex\]](#).
 - [6] E. Aprile *et al.* (XENON), Dark Matter Search Results from a One Ton-Year Exposure of XENON1T, *Phys. Rev. Lett.* **121**, 111302 (2018), [arXiv:1805.12562 \[astro-ph.CO\]](#).
 - [7] P. Agnes *et al.* (DarkSide), DarkSide-50 532-day Dark Matter Search with Low-Radioactivity Argon, *Phys. Rev. D* **98**, 102006 (2018), [arXiv:1802.07198 \[astro-ph.CO\]](#).
 - [8] R. Ajaj *et al.* (DEAP), Search for dark matter with a 231-day exposure of liquid argon using DEAP-3600 at SNOLAB, *Phys. Rev. D* **100**, 022004 (2019), [arXiv:1902.04048 \[astro-ph.CO\]](#).
 - [9] G. Adhikari *et al.* (COSINE-100), Strong constraints from COSINE-100 on the DAMA dark matter results using the same sodium iodide target, *Sci. Adv.* **7**, abk2699 (2021), [arXiv:2104.03537 \[hep-ex\]](#).
 - [10] K. Abe *et al.* (XMASS), Direct dark matter searches with the full data set of XMASS-I, [arXiv:2211.06204 \[astro-ph.CO\]](#).
 - [11] J. Aalbers *et al.* (LZ), First Dark Matter Search Results from the LUX-ZEPLIN (LZ) Experiment,

- arXiv:2207.03764 [hep-ex].
- [12] E. Aprile *et al.* (XENON), First Dark Matter Search with Nuclear Recoils from the XENONnT Experiment, arXiv:2303.14729 [hep-ex].
- [13] J. Angle *et al.* (XENON10), A search for light dark matter in XENON10 data, *Phys. Rev. Lett.* **107**, 051301 (2011), [Erratum: *Phys.Rev.Lett.* 110, 249901 (2013)], arXiv:1104.3088 [astro-ph.CO].
- [14] R. Essig, A. Manalaysay, J. Mardon, P. Sorensen, and T. Volansky, First Direct Detection Limits on sub-GeV Dark Matter from XENON10, *Phys. Rev. Lett.* **109**, 021301 (2012), arXiv:1206.2644 [astro-ph.CO].
- [15] R. Essig, T. Volansky, and T.-T. Yu, New Constraints and Prospects for sub-GeV Dark Matter Scattering off Electrons in Xenon, *Phys. Rev. D* **96**, 043017 (2017), arXiv:1703.00910 [hep-ph].
- [16] E. Aprile *et al.* (XENON), Low-mass dark matter search using ionization signals in XENON100, *Phys. Rev. D* **94**, 092001 (2016), [Erratum: *Phys.Rev.D* 95, 059901 (2017)], arXiv:1605.06262 [astro-ph.CO].
- [17] P. Agnes *et al.* (DarkSide), Low-Mass Dark Matter Search with the DarkSide-50 Experiment, *Phys. Rev. Lett.* **121**, 081307 (2018), arXiv:1802.06994 [astro-ph.HE].
- [18] P. Agnes *et al.* (DarkSide), Constraints on Sub-GeV Dark-Matter–Electron Scattering from the DarkSide-50 Experiment, *Phys. Rev. Lett.* **121**, 111303 (2018), arXiv:1802.06998 [astro-ph.CO].
- [19] E. Aprile *et al.* (XENON), Light Dark Matter Search with Ionization Signals in XENON1T, *Phys. Rev. Lett.* **123**, 251801 (2019), arXiv:1907.11485 [hep-ex].
- [20] E. Aprile *et al.* (XENON), Search for Light Dark Matter Interactions Enhanced by the Migdal Effect or Bremsstrahlung in XENON1T, *Phys. Rev. Lett.* **123**, 241803 (2019), arXiv:1907.12771 [hep-ex].
- [21] C. Cheng *et al.* (PandaX-II), Search for Light Dark Matter–Electron Scatterings in the PandaX-II Experiment, *Phys. Rev. Lett.* **126**, 211803 (2021), arXiv:2101.07479 [hep-ex].
- [22] P. Agnes *et al.* (DarkSide), First Results from the DarkSide-50 Dark Matter Experiment at Laboratori Nazionali del Gran Sasso, *Phys. Lett. B* **743**, 456 (2015), arXiv:1410.0653 [astro-ph.CO].
- [23] P. Agnes *et al.* (DarkSide), Results From the First Use of Low Radioactivity Argon in a Dark Matter Search, *Phys. Rev. D* **93**, 081101 (2016), [Addendum: *Phys.Rev.D* 95, 069901 (2017)], arXiv:1510.00702 [astro-ph.CO].
- [24] P. Agnes *et al.* (DarkSide-50), Search for low-mass dark matter WIMPs with 12 ton-day exposure of DarkSide-50, *Phys. Rev. D* **107**, 063001 (2023), arXiv:2207.11966 [hep-ex].
- [25] P. Agnes *et al.* (DarkSide), Search for Dark-Matter–Nucleon Interactions via Migdal Effect with DarkSide-50, *Phys. Rev. Lett.* **130**, 101001 (2023), arXiv:2207.11967 [hep-ex].
- [26] P. Agnes *et al.* (DarkSide), Search for Dark Matter Particle Interactions with Electron Final States with DarkSide-50, *Phys. Rev. Lett.* **130**, 101002 (2023), arXiv:2207.11968 [hep-ex].
- [27] P. Agnes *et al.* (DarkSide-50), Search for low mass dark matter in DarkSide-50: the bayesian network approach, *Eur. Phys. J. C* **83**, 322 (2023), arXiv:2302.01830 [hep-ex].
- [28] P. Agnes *et al.* (DarkSide), The veto system of the DarkSide-50 experiment, *JINST* **11** (03), P03016, arXiv:1512.07896 [physics.ins-det].
- [29] M.-M. Bé, V. Chisté, C. Dulieu, X. Mougeot, V. Chechev, F. Kondev, A. Nichols, X. Huang, and B. Wang, *Table of radionuclides (Vol. 7 - A = 14 to 245)*, edited by B. I. des Poids et Mesures, Table of radionuclides, Vol. 7 (2013).
- [30] P. Agnes *et al.* (DarkSide), Calibration of the liquid argon ionization response to low energy electronic and nuclear recoils with DarkSide-50, *Phys. Rev. D* **104**, 082005 (2021), arXiv:2107.08087 [physics.ins-det].
- [31] J. Chen, Nuclear Data Sheets for A=39, *Nucl. Data Sheets* **149**, 1 (2018).
- [32] M.-M. Bé, V. Chisté, C. Dulieu, E. Browne, V. Chechev, N. Kuzmenko, R. L. Helmer, A. Nichols, E. Schönfeld, and R. Dersch, *Table of radionuclides (Vol. 1 - A = 1 to 150)*, edited by B. I. des Poids et Mesures, Table of radionuclides, Vol. Vol. 1 - A = 1 to 150 (2004).
- [33] M.-M. Bé, V. Chisté, C. Dulieu, E. Browne, C. Baglin, V. Chechev, N. Kuzmenko, R. L. Helmer, F. Kondev, and T. D. Macmahon, *Table of radionuclides (Vol. 3 - A = 3 to 244)*, edited by B. I. des Poids et Mesures, Vol. 3 (2006).
- [34] P. Agnes *et al.* (DarkSide), Simulation of argon response and light detection in the DarkSide-50 dual phase TPC, *JINST* **12** (10), P10015, arXiv:1707.05630 [physics.ins-det].
- [35] X. Mougeot and C. Bisch, Consistent calculation of the screening and exchange effects in allowed β^- transitions, *Phys. Rev. A* **90**, 012501 (2014).
- [36] S. J. Haselschwardt, J. Kostensalo, X. Mougeot, and J. Suhonen, Improved calculations of beta decay backgrounds to new physics in liquid xenon detectors, *Phys. Rev. C* **102**, 065501 (2020), arXiv:2007.13686 [hep-ex].
- [37] G. Adhikari *et al.* (COSINE-100), Three-year annual modulation search with COSINE-100, *Phys. Rev. D* **106**, 052005 (2022), arXiv:2111.08863 [hep-ex].
- [38] J. Amare *et al.*, Annual modulation results from three-year exposure of ANAIS-112, *Phys. Rev. D* **103**, 102005 (2021), arXiv:2103.01175 [astro-ph.IM].
- [39] E. Aprile *et al.* (XENON), Search for Electronic Recoil Event Rate Modulation with 4 Years of XENON100 Data, *Phys. Rev. Lett.* **118**, 101101 (2017), arXiv:1701.00769 [astro-ph.CO].
- [40] D. S. Akerib *et al.* (LUX), Search for annual and diurnal rate modulations in the LUX experiment, *Phys. Rev. D* **98**, 062005 (2018), arXiv:1807.07113 [astro-ph.CO].
- [41] C. McCabe, The Earth’s velocity for direct detection experiments, *JCAP* **02**, 027, arXiv:1312.1355 [astro-

- ph.CO].
- [42] C. A. J. O'Hare, N. W. Evans, C. McCabe, G. Myeong, and V. Belokurov, Velocity substructure from Gaia and direct searches for dark matter, *Phys. Rev. D* **101**, 023006 (2020), [arXiv:1909.04684 \[astro-ph.GA\]](#).
- [43] J. T. VanderPlas, Understanding the Lomb-Scargle Periodogram, *ApJS* **236**, 16 (2018), [arXiv:1703.09824 \[astro-ph.IM\]](#).
- [44] P. Agnes *et al.* (Global Argon Dark Matter), Sensitivity projections for a dual-phase argon TPC optimized for light dark matter searches through the ionization channel, *Phys. Rev. D* **107**, 112006 (2023), [arXiv:2209.01177 \[physics.ins-det\]](#).
- [45] C. E. Aalseth *et al.* (DarkSide-20k), DarkSide-20k: A 20 tonne two-phase LAr TPC for direct dark matter detection at LNGS, *Eur. Phys. J. Plus* **133**, 131 (2018), [arXiv:1707.08145 \[physics.ins-det\]](#).
- [46] D. Franco *et al.*, Solar neutrino detection in a large volume double-phase liquid argon experiment, *JCAP* **08**, 017, [arXiv:1510.04196 \[physics.ins-det\]](#).